Smart Molecularly Imprinted Polymer Based on Liquid Crystals for Herbicide Recognition

Nouria Bouchikhi, Djahida Lerari, Faycal Dergal, Olivier Soppera, Ouahiba Beladghame, Ulrich Maschke, Khaldoun Bachari, Lamia Bedjaoui-Alachaher

Smart Molecularly Imprinted Polymer Based on Liquid Crystals for Herbicide Recognition

Nouria Bouchikhi[1,2*], Djahida Lerari[1], Faycal Dergal[1,3], Olivier Soppera[4], Ouahiba Beladghame[2], Ulrich Maschke[5], khaldoun Bachari[1] and Lamia Bedjaoui-Alachaher[2]

[1]*Centre de Recherche Scientifique et Technique en Analyses Physico-Chimiques (CRAPC). BP 384, zone industrielle 42004 Tipaza, Algérie*

[2]*Laboratoire de recherche sur les macromolécules (LRM), Université Aboubekr Belkaïd de Tlemcen (UABT), BP119, 13000 Tlemcen, Algérie.*

[3]*Laboratoire (LCSCO), Université de Tlemcen, (UABT), BP119, 13000 Tlemcen, Algérie.*

[4]*Université de Haute-Alsace, CNRS, IS2M UMR 7361, F-68100 Mulhouse, France*

[5]*Unité Matériaux et Transformations UMET (UMR CNRS N°8207), Bâtiment C6, Université de Lille - Sciences et Technologies, 59655 Villeneuve d'AscqCedex, France*

nouria.bouchikhi21@gmail.com*

lerari_zinai@yahoo.fr

dergalf@yahoo.fr

olivier.soppera@uha.fr

wahiba.chimie@yahoo.com

ulrich.maschke@univ-lille1.fr

bachari2000@yahoo.fr

l_bedjaoui@yahoo.fr

Smart Molecularly Imprinted Polymer Based on Liquid Crystals for Herbicide Recognition

This study focuses on the development and characterization of molecularly imprinted thin films in the absence and presence of a liquid crystal monomer, as well as the evaluation of these materials for recognition of the herbicide 2,4-dichlorophenoxyacetic acid (2,4-D). Molecular imprinted polymers (MIPs) and non-imprinted polymers (NIPs) were prepared by using two functional monomers, n-butylmethacrylate (BMA) and liquid crystalline (LC) 6-(4-cyanophenyl-4'phenoxy) hexyl acrylate (A6OCB). The resulting (MIPs) and (NIPs) materials were characterized by infra-red spectroscopy (FTIR), Raman spectroscopy, polarized optical microscopy (POM) and atomic force microscopy (AFM). The entire monomer consumption, as well as the successful loading and extraction of the 2,4-D molecules, were validated by FTIR and Raman analyses. POM and AFM characterization revealed that the percentage of liquid crystal influenced the distribution of the liquid crystal domains, and that the MIP films exhibited remarkable porosity. The experimental results revealed that the MIP films had a substantially higher adsorption capacity towards 2,4-D than the NIP materials, and that increasing the liquid crystal content increased the adsorption capacity of both the MIP and NIP films. The selectivity tests in the presence of phenoxyacetic acid (POAc) showed that the MIP films exhibited higher affinity for 2,4-D than for the POAc.

Keywords: Imprinted polymer, liquid crystal, recognition capacity, selectivity factor, 2,4-D extraction.

1. Introduction

2,4-D, a member of the phenoxyacid herbicide family, is widely used to control weed growth. However, the use of this pesticide, while required for crop protection, poses a risk due to the contamination that it causes in the food supply and the environment. As a result of its heavy use, 2,4-D residues have been found in environmental waters, fresh vegetables, and dairy products. [1-3] Therefore, the detection of low amounts of 2,4-D in soil and natural waters has been a challenge for researchers in recent years. Many approaches have been used to monitor 2,4-D residue in the environment, including high performance liquid chromatography (HPLC), gas chromatography-mass spectrometry (GC/MS), [4-6] electrochemical sensor [7,8] and solid-phase extraction. [9,10] Due to the intricacy of the sample matrices and the low 2,4-D concentration, these approaches frequently necessitate significant sample preparation and separation operations. They also have several drawbacks, such as sophisticated instrumentation, expensive costs, a time-consuming process and low selectivity. Molecular imprinting (MIP) technology, which has focused on the ability to create molecular recognition sites with high adsorption selectivity and binding capacity for the target molecule, is one of the most promising technologies for the development of highly selective functional materials. [11,12] A brief review of the literature reveals that MIP technology has received considerable attention for its use in 2,4-D detection due to its high recognition capacity and specificity. [13-15]

Molecularly imprinted polymers (MIPs) are commonly synthesized in practice by copolymerizing a functional monomer with a cross-linking monomer through a radical polymerization mechanism in the presence of a target molecule that acts as a molecular template. The functional monomer first forms a complex with the template molecules via covalent or non-covalent bonds before the photo-crosslinking process. Following template

removal, specific binding sites that are complementary in size and shape to the target molecule are left. [16,17]

To avoid cavity deformation after template extraction, the binding sites must be preserved by stiffening the polymeric network. Polymer rigidity can be increased by increasing the amount of crosslinker in the polymerization mixture (usually around 80-95 percent). [18] Otherwise, it has been found that in the case of a non-covalent approach, only 15 to 20% of the imprinted sites can load the template molecules, which is attributed to the high level of crosslinking which can cause the collapse of formed cavities. [19, 20]

To address this issue efforts have been made to balance the stiffness and flexibility of the polymeric network, including the use of controlled radical polymerization, [21,22] crowding agents [23-25] and the incorporation of liquid crystal (LC) monomers into the polymer matrix. [26-28] This latter approach is based on replacing chemical crosslinking with physical crosslinking provided by the interaction of the mesogenic side groups. Furthermore, using LC monomers in the synthesis of MIP materials can soften the polymeric network and add complementary functionalities at the same time, which can improve accessibility and prevent cavities from shrinking.

Mauzac et al. used this technique to successfully prepare low crosslinked polysiloxane (5-20 mol% of the 1,21-docosadiene used as a crosslinking agent) imprinted polymers in which the interaction between mesogenic moieties ensured that chemical crosslinking was replaced by physical crosslinking. [29-31] Using the same strategy, Wei et al. prepared an LC-MIP coating for chiral separation of enantiomers for the first time. The resulting low crosslinked (20%), open-tubular imprinted capillary was able to separate enantiomers using capillary electrochromatography (CEC). [20] These encouraging results demonstrating the benefit of liquid crystal monomer insertion have recently garnered the curiosity of several research

groups with the aim of improving the usefulness of LC-MIP in several fields, such as drug delivery control, stationary phase for CEC, HPLC [26,32,33] and for fabrication of sensors. [34,35] MIPs materials are traditionally prepared as monoliths for use as stationary phases or as thin films for sensing applications. MIP thin films are frequently produced using the sandwich or spin coating methods. Despite the numerous advantages of using MIP-based thin films in sensing, the need to increase accessibility and sensitivity remains important. To that end, LC-MIP thin films have been developed by Yun et al, to improve sensor performance. Their findings demonstrated the potential of the obtained LC-MIP for use in biomaterials and sensing. [36]

Given the facts stated above, the use of LC-MIP in sensitive materials should provide new opportunities in the field of pollutant adsorption and detection. The objective of this study was to demonstrate the effect of LC moieties insertion in MIPs films for 2,4-D recognition. A comparative study was conducted to compare the high crosslinker MIP thin films to two other films containing 20 mol% and 50 mol% LC monomer with low crosslinker content. AT-FTIR, Raman, POM, and AFM techniques were used to characterize the resulting polymer films, and batch rebinding experiments were used to highlight the adsorption capacities of each polymer. The novelty of this study is to the presentation of the advantages of inserting LCs into weakly cross-linked MIPs that can selectively bind the herbicide 2,4-D.

2. Experimental section

2.1 Reagents and chemicals

The liquid crystal monomer 6-(4'-cyanophenyl-4''-phenoxy) hexyl acrylate (A-6OCB) was obtained from Synthon Chemicals GmbH & *Co* KG, Germany; n-butyl methacrylate (BMA > 98%), 1,6 hexanedioldiacrylate (HDDA> 98%), 2,4-dichlorophenoxyacetic acid (2,4-D 97%), phenoxyaceticacid (POAc 98%), ethanol (99%) and acetonitrile (ACN 99%) were purchased from Sigma-Aldrich Co. Inc, USA and used as received. The photo-initiator 2-hydroxy-2-

methyl-1-phenyl-1-propanone (Darocur 1173) was supplied by Ciba- Geigy Co. Switzerland. The chemical structures of all reactants are illustrated in Fig.1.

Figure 1

2.2 Instrumentation

Fourier transform infra-red (FTIR) analyses were recorded using an Agilent Cary 640 instrument spectrometer Agilent Technology Co. USA. Spectra were recorded over the range of 4000-400 cm^{-1} with accumulated and averaged 32 scans and a resolution of 2 cm^{-1}.

Raman spectroscopic investigations were performed using a Raman spectrometer (HORIBA Ltd. France S.A.S.) operated in single spectrograph mode with a holographic dispersive grating of 600 grooves/mm and equipped with a 633, 785 and 325 nm He-Ne lasers. The samples were analyzed in the back-scattering mode on the microscope stage of an Olympus confocal microscope (Horriba Ltd, Japan) attached to the spectrometer using a long working distance 50× objective. The detector used was a liquid nitrogen cooled charge coupled device Symphony IGA detector (Horriba Ltd, Japan). 663 and 785 nm holographic notch filters were used to remove the Rayleigh-scattered light. The entrance slit width was 100 μm, giving a resolution of 2 cm^{-1} in the range between 100 and 5000 cm^{-1}. Repeated acquisitions using the highest magnification were accumulated and averaged to improve the signal to noise ratio in the spectra. The spectra were calibrated using the 520.5 cm^{-1} line of a silicon wafer.

Polarizing optical microscopy (POM) observations were conducted on a BX41, Olympus Co. Japan microscope equipped with a camera to taking pictures.

Atomic force microscopy (AFM) analysis of the thin films was conducted using a Flex- AFM (nanosurf Co. Switzerland), operated in the tapping mode. The scanning head was connected to a C3000 controller (nanosurf Co. Switzerland) working at resonance frequencies < 4 MHz. The Flex AFM video option integrates two cameras for a parallel top and side view, which allows quickly finding an area of interest and bringing the cantilever closer to the surface

before the final approach. An area of 4x4 µm² size was scanned for all samples and the obtained images were treated by using the image processing Gwyddion software (nanosurf Co. Switzerland). UV analysis, were performed on a Specord 200 plus Analytik Jena GmbH+Co.KG Germany, using quartz cells.

2.3 Polymer films preparation

Polymer thin films preparation was carried out by the free-radical photo-polymerization of the monomers (BMA and A6OCB), using HDDA as a crosslinker, in the presence of Darocur as a photoinitiator and ACN as a solvent. For the MIPs preparation, a fixed amount, as described below of 2,4-D template was added to the formulations.

In order to underline the impact of liquid crystal insertion on the properties and binding capacities of the materials, three sets of formulations were prepared and characterized, by varying the monomers ratio. The compositions of the precursor solutions are listed in Table1. The solvent (acetonitrile) was added at a 3:4 ratio (volume of monomers (ml): volume of solvent (ml)). The amount of the photo-initiator was 1mol% of the total moles number of monomers used. In the absence of A6OCB, the molar ratio (template/monomer/crosslinking agent) was (1/4/20), while in its presence; it was (1/4/4).

Table 1

In this study the preparation of the NIPs and MIPs polymer films was achieved by a sandwich method. For this, 200µL of the mixture was deposited on a glass slide with a thickness spacer (130µm). To avoid the solvent evaporation and oxygen inhibition, a film of PET with a thickness of 23µm was placed on the mixture. The mixture was then irradiated by UV irradiation (Lg.Philips Lcd Co., Ltd South Korea, λ =365 nm, I_0=0.7 mw/cm^2). Transparent thin films with a thickness of 100 µm were obtained; the film thickness was measured by means of a micrometer model 103–137 (Mitutoyo Europe GmbH, Germany) with an accuracy of 0.001 mm, taking the average at five different points of the film. The obtained MIPs films

were carefully washed with acetonitrile: ethanol (9:1v/v) in order to extract the 2,4-D molecules. The washed MIPs films were then recovered and dried.

2.4 Rebinding experiments

For the adsorption tests 4mg of NIP and MIP polymer films were immersed separately in 1mL of 2,4-D solution at a concentration of 1mg/ml. The mixture was shaken for 2h at 25°C and the supernatant was then analyzed by UV at 284nm to measure the adsorption of each system. All experiments were conducted for four times, and the average value was used.

The amount of 2,4-D adsorbed in the NIPs and MIPs films at equilibrium was calculated according to the following equation.

$$Q = \frac{(C_i - C_f)V}{m} \qquad (1)$$

Where:

Q is the binding capacity of the films, (mg of 2,4-D / g of film).

C_i (g/L) and C_f (g/L) are the initial and final concentrations of 2,4-D.

V (L) is the initial volume of the solution.

m (g) is the mass of the polymer film.

In order to evaluate the adsorbed amount of 2,4-D in the binding experiments, a calibration curve relating absorbance to 2,4-D concentration was prepared with a regression coefficient of 0.998. The imprinting effect illustrated by the IF values was calculated as the ratio of the MIP binding capacity (QMIP) to that of the non-imprinted polymer (Q_{NIP}). For each rebinding test, the imprinting factor (IF) was calculated.

$$IF = \frac{Q_{WMIP}}{Q_{NIP}} \qquad (2)$$

2.5 Selectivity studies

The selectivity of the MIPs systems was evaluated in the presence of phenoxyacetic acid (POAc) as a structurally related compound; for this, 4mg of MIP film was incubated in 1ml of POAc at a concentration of 1mg/ml for 2 hours. The supernatant was then analyzed by UV and the capacity was calculated by monitoring the absorbance at 271nm with the POAc concentration determined by using a calibration curve established for the POAc molecule with a regression coefficient of 0.999.

The Selectivity factor (α) of the imprinted polymer was calculated as the ratio of POAc to 2,4-D bound to the imprinted polymer. [37]

$$\alpha = \frac{Q(POA)}{Q(2,4-D)} \qquad (3)$$

Where Q (POAc) and Q (2,4-D) are the bound amounts of POAc and 2,4-D for the MIP, respectively.

3. Results and discussion

3.1 Polymer films characterization

3.1.1 ATR-FTIR

Figure 2 depicts the infrared spectra of BMA, A6OCB, and the obtained NIPs films.

Figure 2

The BMA and A6OCB spectra (Fig. 2a) showed some common peaks; the strong absorption peak at 1716 cm^{-1} is assigned to the carbonyl group (C=O). The peaks at 1159 cm^{-1} and 1295 cm^{-1} are attributed to C-O groups and the peaks at 1635$cm^{-1}$and 810 cm^{-1} are related to the C=C function. The C-H elongation appears at 2940 cm^{-1} . [38] The BMA spectrum differs from that of the A6OCB by the appearance of a band at 940cm^{-1}. This is assigned to the out of plane CH bending vibrations of the disubstituted C=C bond. The peak that appears at 2223 cm^{-1} in the A6OCB spectrum is assigned to the CN group.

In the FTIR spectra of the polymers (Fig. 2b), the photo-crosslinking was confirmed by the disappearance of the C=C double bond peaks at 1635cm^{-1} and 810 cm^{-1}, respectively. A shift in the C=O stretching peak was also noted, from 1716 to 1725 cm^{-1}, which could be attributed to the loss of conjugation following the photo-crosslinking reaction. [39,40] A simple comparison of the NIP1 films spectra with those of NIP2 and NIP3 shows the presence of characteristic peaks of the liquid crystal monomer in the spectra of NIP2 and NIP3 at 2223 cm^{-1}, related to the CN stretching, and at 1601 cm^{-1} and 824cm^{-1} attributed to the aromatic C=C stretching and aromatic C-H deformation, respectively.

For a better illustration of the 2,4-D loading in the imprinted polymers, the 2,4-D and MIPs films were characterized by FTIR analysis and the obtained spectra are shown in Fig. 3.

Figure 3

The FT-IR spectrum of 2,4-D displays a peak at 1715 cm^{-1} indicating the presence of carboxyl groups, the bands at 1310 cm^{-1} and 1087 cm^{-1} are due to the antisymmetric and symmetric vibrations of C-O-C and the peak located at 1234 cm^{-1} is attributed to the O-H deformation coupled with C-O stretching. [41] The peaks at 1477 cm^{-1} and 1601 cm^{-1}are related to C=C vibrations of the aromatic ring. The characteristic band of C-Cl stretching occurs at 694 cm^{-1}. The band located at 791 is attributed to C-H deformation of the aromatic rings and the band at 3019 cm^{-1} represents OH stretching vibrations.

The characteristic 2,4-D peaks at 1601 cm^{-1} and 791 cm^{-1} in the spectrum of the MIP1 polymer can hardly be visualized; while in the case of the MIP2 and MIP3 films, we note the appearance of the peak at 1601 cm-1 which can be attributed to the aromatic C=C bond of the template (2,4-D) and the monomer (A6OCB) due to the overlap of the 2,4-D and A6OCB peaks in this region. The presence of peaks at 2223 cm^{-1}, 1601 cm^{-1} and 824 cm^{-1}in the MIP2 and MIP3 spectra confirms the presence of the A6OCB monomer in these films. It is possible to observe that the FTIR spectra of the NIP films (Fig. 2b) and MIP films (Fig. 3b) show

similar characteristic absorption bands, indicating a similarity in the backbone structure of the different polymers. It is also possible to observe that the intensities of the characteristic A6OCB peaks are greater in the case of MIP3 compared to those of MIP2 ones, indicating that MIP3 films have a higher A6OCB content.

3.1.2 Raman spectroscopy

In order to provide more information about the insertion of LC monomer and 2,4-D within the MIPs materials, Raman spectroscopy was used in this work. Figure 4 depicts the Raman spectra of A6OCB, NIP1, NIP2 and NIP3, respectively.

Figure 4

Raman spectrum of A6OCB (Fig. 4a) shows a strong absorption peak at 1606 cm^{-1} and 824 cm^{-1}that are assigned to the aromatic C=C stretching and C-H deformation, respectively. The peaks at 1178 cm^{-1} and 1290 cm^{-1} are attributed to C-O groups. The peak that appears at 2225 cm^{-1} in the A6OCB spectrum is assigned to the CN group.

The Raman Spectra of the NIPs polymers, as shown in Fig. 4b, are identical expect for the existence of A6OCB characteristic bands in the spectra of NIP2 and NIP3 at 2225 cm-1, related to the CN stretching vibrations, and at 1602 cm^{-1} and 838 cm-1, that are attributed to the aromatic C=C stretching vibrations and aromatic C-H deformation, respectively.

Raman spectroscopy was also used to characterize the MIPs films in order to confirm the success of 2,4-D loading in the imprinted polymers during the polymerization process; the obtained spectra are shown in Fig. 5.

Figure 5

The Raman bands of 2,4-D (Fig. 5a), detected at 412 and 647 cm^{-1} are related to the in-plane vibrational modes of the C-O-C and C-Cl bonds. The band at 719 $cm^{-1}$is referred to the bending of COO plus the stretching of aromatic C-C. the stretching of aromatic C-C plus C-O plus C-Cl, noted as ν(CC)ring + ν (C-O)+ ν (C-Cl) appears at 839 cm^{-1} and the band at 894

cm^{-1} is related to the stretching of the C-COO bonds. The bands at 1162 cm^{-1} and 1260 cm^{-1} are due to the symmetric and antisymmetric bending of the aromatic CH bonds plus the stretching of the C-O bond. The Raman band at 1446 cm^{-1} is assigned to the symmetric stretching of COO plus the stretching of CC plus the wagging of CH_2, and the band located at 1160 cm^{-1} has been attributed to the O-H deformation coupled with C-O stretching. The band located at 1595 cm^{-1} is attributed to the antisymmetric stretching of COO plus stretching of aromatic C-C. [42]

The Raman spectra of the MIPs films depicted in Fig. 5b, show similar characteristic absorption bands, indicating similarity in the backbone structure of the different obtained polymers. In the case of MIP2 and MIP3, characteristic A6OCB peaks appear at 2225 cm^{-1}, 1602 cm^{-1} and 838 cm^{-1}, related to CN stretching vibrations, aromatic C=C stretching vibrations and aromatic C-H deformation, respectively. The insertion of 2,4-D into MIP films was easier to observe by the Raman technique than by the FTIR technique. From Fig. 5b, the characteristic 2,4-D peaks at 1602 $cm^{-1}$and 838cm^{-1} in MIP2 and MIP3 polymers correspond to the aromatic C=C and CH bonds and can be attributed to both the template (2,4-D) and the monomer (A6OCB) due to overlapping of 2,4-D and monomers peaks in this region. The presence of 2,4-D can be distinguished by the appearance of the characteristic bands of the C-Cl bond that appear at 649 cm^{-1} and 412 cm^{-1} particularly in the MIP2 and MIP3 spectra (Fig. 5c). Due to the low concentration of 2,4-D in the presence of a high crosslinker content in MIP1, these peaks are barely apparent when compared to the spectra of MIP2 and MIP3.

To assess the effectiveness of the washing process the MIP1 film was analyzed by Raman spectroscopy before and after several washes. Figure 6 shows the spectra of 2,4-D, MIP1 and washed MIP1 as a typical example around the characteristic 2,4-D peaks at 646cm^{-1} and 412 cm^{-1}.

Figure 6

Figure 6 indicates that the characteristic bands of 2,4-D at 412 cm^{-1} and 646 cm^{-1}, clearly appear in the spectra of MIP1 and disappear in that of the washed MIP1. This result suggests that the 2,4-D was successfully incorporated in MIP films during polymerization and released during several washes.

In the following we will describe the characterization of MIP2 and MIP3 films by Raman imaging. XY (2D) Raman mapping experiments were performed to determine the distribution of liquid crystal clusters in the polymer matrix. The mapping results were expressed in terms of the BMA, A6OCB and 2,4-D characteristic peaks at 1373 cm-1, 2225 cm^{-1} and 647 cm^{-1} for BMA, A6OCB and 2,4-D, respectively. [43] The selected peaks must exist in only one of the components of the mixture. This parameter proved to be adequate to study the spatial distribution of the liquid crystal monomer in the BMA matrix. The selected peaks were 1373 cm^{-1} related to the CH_3 stretching vibrations of the BMA methacrylate in red color, and 2225 cm^{-1} of the liquid crystal representing CN stretching vibrations in blue color (Fig. 7). Raman mapping was performed on an image taken with a ×100 magnification of the polymer on a 900 μm^2 for MIP2 and 1800 for MIP3 μm^2 surface. Figure 7 shows the results of the XY mapping of MIP2 and MIP3 expressed in terms of their characteristic peaks.

Figure 7

From the mapping plots, when we compare the distribution of BMA (red color) to that of A6OCB (blue color) most of the area was overlapped. Accordingly, the presence and the localization of the liquid crystals clusters were not homogeneous and the distribution was completely random.

The comparison between the obtained Raman mappings shows an increase in the size of the blue areas in the case of MIP3 which contained a significant amount of LC; these observations can confirm the results obtained by FTIR indicating the increase in peak intensity and LC cluster size with the increase in the amount of LC. Mapping was also used to

highlight the insertion of 2,4-D molecules into the polymer matrix. For this, the characteristic peak of 2,4-D at 647 cm^{-1} was used to show XY mapping. The presence of 2,4-D is illustrated by green color in the mapping images. The result suggests that 2,4-D molecules are localized near the A6OCB domains which can be explained by the strength of hydrogen bonding between the 2,4-D and A6OCB monomers.

3.1.3 POM characterization

To better see the distribution of the mesogenic parts in the NIPs and MIPs films, a morphological study was performed by an Olympus BX41 polarizing microscope with a camera used for the observation of the phases present in the polymer film. Optical micrographs of each sample were taken under both parallel and crossed polarizers with a 20x magnification at room temperature. The micrographs presented in Fig. 8 show the textures observed for the NIPs and MIPs films. The left-hand column of Fig. 8 depicts micrographs taken with a parallel polarizer, while the right-hand column depicts micrographs taken with a crossed polarizer; thus, the anisotropic nature of the LC parts was confirmed under cross-polarization, as they appear colored.

Figure 8

It can be seen that the mesogenic domains are easily distinguished in the systems obtained in the presence of A6OCB. Indeed, we can see a clear difference in the size and distribution of these domains in the polymeric networks as a function of A6OCB concentration. The domains grow in size as the amount of A6OCB increases. It is also worth noting that the distribution of the CLs domains was not uniform across the networks due to the fact that it is a statistical copolymer.

3.1.4 AFM characterization

The AFM results shown below are for the BMA/HDDA systems in the absence and presence of A6OCB. Since AFM is a localized analysis technique, it could give an accurate representation of the polymer surface after the 2,4-D was removed by washing. Then the MIPs films were characterized after several washes. Figure 9 depicts the topographies of the films surfaces over an area of 4x4 μm^2.

Figure 9

The color density shows the vertical profile of the sample with the darkest regions representing the pores and the lightest regions representing the peaks.

To quantitatively evaluate the roughness properties, three roughness parameters were used in relation to the cross-section profiles of the surface, including average roughness (Ra), root mean squared roughness (RMS), and Maximum peak to valley height (Rmax), this later is is defined as the maximum peak-to-valley height within any of the sampling lengths of the profile. For this purpose, the images of the polymer thin films obtained by AFM were treated by using the image processing Gwyddion software.

After the topoghraphy was plotted an arbitrary straight line was drawn on the image and the specific roughness was analyzed on the defined trace; for this, seven horizontal cross-sectional lines were drawn, examined and the roughness values were averaged. The measurement results of the sample roughness in the experiment are shown in Table 2.

Table 2

The 3D topography images show that both the MIPs and NIPs films displayed rough surfaces. By comparing the topographies of the MIPs and NIPs films for all formulations, it can be seen

that in the case of the MIPs films, a porous structure was created after template removal whereas for the NIPs films the surface was less porous.

The roughness observed in the surface topography reveals cavities that could be attributed to the imprinting of 2,4-D in the polymer matrix. [44,45] These observations are promising for the success of molecular imprinting and also provided evidence that the washing process could remove 2,4-D molecules from the polymer film.

Roughness analysis (see Table2) indicates that the MIPs films were relatively harsh with significant surface roughness. It's noted that the NIPs films were also rough but their average roughnesses were remarkably lower than those obtained for the MIPs films.

Furthermore, the obtained values showed that the surface roughness of the MIP films was evenly distributed across the entire surface, and the molecular imprinting process was effectively completed.

The data shown on Table 2 also indicate that, after the template was removed, the depth of pores increased as the crosslinking density decreased. This finding is most likely due to an increase in template concentration in the presence of low crosslinker content, which results in the formation of wide pores.

3.2 Rebinding studies

MIPs, like other adsorbents, can be classified based on their recognition properties. This latter point is critical because the primary goal of a MIP preparation is adsorption. The recognition tests were carried out after the template molecules were extracted to their maximum extent. The ability of a MIP to recognize and, in practice, re-adsorb the molecule for which it is produced is used to evaluate its recognition properties.

Binding tests were used in this study to characterize the recognition properties of the MIPs, which were investigated by incubating 4 mg of washed MIP or NIP films in template solution

at a concentration of 1mg/ml for 2 hours. Most studies have found that when a porogen was used as a binding solvent, higher binding capacities were observed. [46,47] For this, acetonitrile was chosen as the solvent for rebinding studies.

The binding properties of the MIPs films were compared to those of the NIPs as controls. Figure 10 depicts the amount of 2,4-D bound to the MIPs and NIPs films in the absence and presence of A6OCB at two molar ratios (20 and 50%, respectively).

Figure 10

In all systems, the imprinted polymer recognized 2,4-D molecules better than the non-imprinted polymer. This higher affinity of the MIP films towards 2,4-D can be attributed to the presence of effective binding sites on the MIP surface, which allows the 2,4-D molecules to diffuse into the MIP pores during rebinding. Further, this result proves that the imprinted polymers keep a memory towards the template molecule.

It is important to note here that in the presence of the liquid crystal monomer, a low level of crosslinking was intentionally targeted to show how physical crosslinking governed by the liquid crystal can replace the chemical crosslinking provided by a high level of crosslinking agent.

The results revealed that the amount of 2,4-D bound to MIP2/NIP2 and MIP3/MIP3 was significantly higher than that bound to MIP1/NIP1. This finding can be attributed to the rigidity of the polymers formed in the presence of high crosslinking density in the case of MIP1/NIP1 which can limit the diffusion of 2,4-D molecules into the polymers. This finding is consistent with other studies showing that the binding capacity of polymers increases as the crosslinking density decreases. [37] However the rigid MIP1 films with high crosslinking density displayed higher specific binding (IF=1.70) than the MIP2 and MIP3 with low IF (IF_{MIP2}=1.14 and IF_{MIP3}=1.10), respectively.

The high selectivity of our rigid polymers is due to the stability of the cavities formed in the presence of a high HDDA content. These results showed that the crosslinking agent was important for the stability of the cavities and the rigidity of the formed polymer. Replacing HDDA by A6OCB, which can provide physical crosslinking due to its mesogenic nature, was insufficient to create a polymer with high specificity.

In the case of MIP2 and MIP3, prepared with two different molar ratios of A6OCB and the same crosslinking density, the binding capacity of the polymer films increased as the A6OCB content increased. These findings confirm that the presence of A6OCB as a co-functional monomer resulted in the formation of more functionalized cavities, as well as that adsorption occurs not only on the cavities formed during polymer formation, but also on the functionalized sites formed by increasing the content of co-functional monomers. It has been reported that it is easier to understand binding and selectivity trends in non-covalently printed polymers when multiple functional monomers are used to create binding sites of higher affinity and selectivity. [48,49]

The results presented in this work demonstrated the potential of the new liquid crystal functional monomer to create binding sites capable of selectively binding 2,4-D molecules. It is clear that the formation of the pre-polymerization complex between the 2,4-D template and the two monomers, BMA and A6OCB was dominated by H-bond type interactions (shown schematically in Fig. 11), which significantly enhances the binding strength of the template-monomer complex and eventually improves the performance of the MIP materials.

Figure 11

3.3 Adsorption selectivity

The recognition selectivity towards the template molecule used in the polymerization stage is the best indicator of the efficacy of imprinted polymers; this selectivity is dependent on the complementary binding sites introduced in the polymer after template removal, as well as the size and shape of the template. Selectivity recognition tests were performed in the presence of the structurally related compound POAc to evaluate the selection ability of the prepared MIPs films towards 2,4-D. The adsorption capacities of the MIPs films towards 2,4-D and POAc at a concentration of 1mg/ml are shown in Fig.12.

Figure 12

The results presented in Fig. 12 indicate that the ability of the polymers to bind to 2,4-D was significantly higher than that of POAc, despite their similar structures, demonstrating a higher selectivity of the obtained MIPs towards 2,4-D.The selectivity factor calculated using Eq3 expresses the degree of selectivity of the imprinted polymers. When 2,4-D is bound to the polymer, the value is one; when POAc is adsorbed, the value is less than one. The selectivity factors of the MIPs that were used are summarized in Table 3.

Table 3

The results show that the selectivity factors were less than one for all studied systems, demonstrating the imprinting efficiency of the imprinted polymers and confirming that not only the functional carboxyl group but also the shape and size of the 2,4-D printed in three-dimensional cavities can govern recognition. This result is consistent with other researchers' findings showing that the substitution in the aromatic ring by chlorine atoms in template molecules increases the recognition capacity of polymers printed by 2,4-D. [50,51]

4. Conclusions

In our research described here, novel MIPs thin films were prepared photo-chemically by a non-covalent imprinting approach for 2,4-D recognition using BMA and liquid crystal

A6OCB as functional monomers, HDDA as a crosslinker and acetonitrile as a porogenic solvent.

The success of polymerization and liquid crystal monomer and template insertion were characterized by means of FTIR and Raman spectroscopy. The morphological and topographic properties of obtained polymers were evaluated using MOP and AFM techniques. The results from MOP indicated that the A6OCB distribution over the polymer was not uniform and the AFM images clearly showed that the size and the depth of pores increased with decreasing the crosslinking density. The recognition ability of MIP was estimated by rebinding experiments using 2,4-D as the original template and POAc as a structurally similar compound. The experimental results revealed that the obtained MIPs exhibited better loading of 2,4-D compared with the NIPs polymers. Furthermore, the presence of liquid crystal monomer enhanced the recognition capacity of both the MIPs and NIPs films. This result can be explained by two factors; the ease of template diffusion by decreasing the cross-linking density and the increase of functional sites within the polymer due to the increase of A6OCB content which can interact with 2,4-D by hydrogen bonding due to the presence of cyano and carbonyl groups. The increase of crosslinking density led to the decrease of adsorption capacity whereas the specificity was increased due to the rigidity of the resulting polymers which can limit the template diffusion and maintains the original cavities formed. Overall, the resulting MIP films showed a good selectivity to 2,4-D molecules. Based on these findings we suggest that the obtained thin films could be useful and efficient in environmental sensors and other applications for selective uptake of 2,4-D.

Declaration of competing interest

The authors declare that they have no known competing financial interests or personal relationships that could have appeared to influence the work reported in this paper.

Acknowledgements

The authors gratefully acknowledge the support of the Algerian Ministry of Higher Education and Scientific Research (MESRS), the General Directorate of Scientific Research and Technological Development (DGRSDT) of Algeria, the CRAPC center, the University of Tlemcen in Algeria, the CNRS and IS2M institute.

References

[1] Kuang, L.; Hou, Y.; Huang, F.; Hong, H.; Sun, H.; Deng, W.; Lin, H. Pesticide residues in breast milk and the associated risk assessment: A review focused on China. *Sci. Total Environ.* **2020**, 727, 138412. DOI: 10.1016/j.scitotenv.2020.138412.

[2] Qu, F.; Lin, L.; Cai, C.; Chu, B.; Wang, Y.; He, Y.; Nie, P. Terahertz finger print characterization of 2, 4-dichlorophenoxyacetic acid and its enhanced detection in food matrices combined with spectral baseline correction. *Food Chem*. **2021**, 334, 127474. DOI: 10.1016/j.foodchem.2020.127474

[3] Li, Z.F.; Dong, J. X.; Vasylieva, N.; Cui, Y. L.; Wan, D. B.; Hua, X. D.; Hammock, B. D. Highly specific nanobody against herbicide 2, 4-dichlorophenoxyacetic acid for monitoring of its contamination in environmental water. *Sci. Total Environ.* **2021**, 753, 141950. DOI: 10.1016/j.scitotenv.2020.141950.

[4] Zhu, X.; Li, J.; Xie, B.; Feng, D.; Li, Y. Accelerating effects of biochar for pyrite-catalyzed Fenton-like oxidation of herbicide 2, 4-D. *Chem. Eng. J.* **2020**, 391, 123605. DOI: 10.1016/j.cej.2019.123605.

[5] Yang, W.; Zhou, M.; Oturan, N.; Li, Y.; Su, P.; Oturan, M. A. Enhanced activation of hydrogen peroxide using nitrogen doped graphene for effective removal of herbicide 2, 4-D from water by iron-free electrochemical advanced oxidation. *Electrochim. Acta* **2019**, 297, 582-592. DOI: 10.1016/j.electacta.2018.11.196.

[6] Zhang, Z.; Ma, X.; Jia, M.; Li, B.; Rong, J.; Yang, X. Deposition of CdTe quantum dots on microfluidic paper chips for rapid fluorescence detection of pesticide 2, 4-D. *Analyst* **2019**, 144, 1282-1291. DOI: 10.1039/C8AN02051E.

[7] Goswami, B.; Mahanta, D. Fe3O4-Polyaniline Nanocomposite for Non-enzymatic Electrochemical Detection of 2, 4-Dichlorophenoxyacetic Acid. *ACS omega* **2021**, 6, 17239-17246. DOI: 10.1021/acsomega.1c00983.

[8] Yang, Y.; O'Riordan, A.; Lovera, P. Highly sensitive pesticide detection using electrochemically prepared Silver-GumArabic nanocluster SERS substrates. Sens. Actuator B-Chem. **2022**, 364, 131851. DOI: 10.1016/j.snb.2022.131851.

[9] Tölgyesi, Á.; Korozs, G.; Tóth, E.; Bálint, M.; Ma, X.; Sharma, V. K. Automation in quantifying phenoxy herbicides and bentazon in surface water and ground water using novel solid phase extraction and liquid chromatography tandem mass spectrometry. Chemosphere **2022,** 286, 131927. DOI: 10. 1016/ j. chemosphere. 2021.131927.

[10] Han,Y.; Wang, Z.; Jia, J.; Bai, L.; Liu, H.; Shen, S.; Yan, H. Newly designed molecularly imprinted 3-aminophenol-glyoxal-urea resin as hydrophilic solid-phase extraction sorbent for specific simultaneous determination of three plant growth regulators in green bell peppers. *Food Chem.* **2020**, 311, 125999. DOI: 10.1016/j.foodchem.2019.125999.

[11] Zhang, K.; Wang, Y.; We, Q.; Huang, Q.; Li, T.; Zhang, Y.; Luo, D. Preparation and characterization of magnetic molecularly imprinted polymer for specific adsorption of wheat gliadin. *J. Mol. Struct.* **2022**, 1265, 133227. DOI: 10.1016/ j.molstruc.2022.133227.

[12] Karuehanon, W.; Funfuenha, W.; Phuttawong, N. Selective triphenylphosphine oxide imprinted polymer for solid scavenger application in organic synthesis *J Chem Sci*. **2022**, 134,21. DOI: 10.1007/s12039-021-02021-1.

[13] Guć, M.; Messyasz, B.; G, Schroeder. Environmental impact of molecularly imprinted polymers used as analyte sorbents in mass spectrometry. *Sci. Total Environ.* **2021**, 772, 145074. DOI: 10.1016/j.scitotenv.2021.145074.

[14] Lee, J.; Yang, J. C.; Lone, S.; Park, W. I.; Lin, Z.; Park, J.; Hong, S. W. Enabling the Selective Detection of Endocrine-Disrupting Chemicals via Molecularly Surface-Imprinted "Coffee Rings". *Biomacromolecules* **2021**, 22, 1523-1531. DOI: 10.1021/acs.biomac.0c01748.

[15] Beladghame, O.; Bouchikhi, N.; Lerari, D.; Charif, I. E.; Soppera, O.; Maschke, U.; Bedjaoui-Alachaher, L. Elaboration and characterization of molecularly imprinted polymer films based on acrylate for recognition of 2, 4-D herbicide analogue. *Iran. Polym. J.* **2023**, 32, 483. DOI: 10.1007/s13726-023-01143-2.

[16] Paruli, E.I.; Soppera, O.; Haupt, K.; Gonzato, C. Photopolymerization and photostructuring of molecularly imprinted polymers. ACS Appl. Polym Mater. **2021,** 3, 4769-4790. DOI: 10.1021/acsapm.1c00661.

[17] Kajisa, T.; Sakata,T. Molecularly imprinted artificial biointerface for an enzyme-free glucose transistor. ACS Appl. Mater. Interfaces **2018**, 10, 34983-34990. DOI: 10.1021/acsami.8b13317.

[18] BelBruno, J. J. Molecularly imprinted polymers. *Chem. Rev.* **2018**, 119**,** 94-119. DOI: 10.1021/acs.chemrev.8b00171.

[19] Suwanwong, Y.; Boonpangrak, S. Molecularly imprinted polymers for the extraction and determination of water-soluble vitamins: A review from 2001 to 2020. Eur. Polym. J. **2021**, 161, 110835. DOI: 10.1016/j.eurpolymj.2021.110835.

[20] Wei, Z. H.; Mu, L. N.; Huang, Y. P.; Liu, Z. S. Low crosslinking imprinted coatings based on liquid crystal for capillary electrochromatography. J. Chromatogr. A **2012**, 1237, 115-121. DOI: 10.1016/j.chroma.2012.03.041.

[21] Ramakers, G.; Wackers, G.; Trouillet, V.; Welle, A.; Wagner, P.; Junkers, T. Laser-grafted molecularly imprinted polymers for the detection of histamine from organocatalyzed atom transfer radical polymerization. *Macromolecules* **2019**, *52*, 2304-2313. DOI: 10.1021/acs.macromol.8b02339.

[22] Montagna, V.; Haupt, K.; Gonzato, C. RAFT coupling chemistry: a general approach for post-functionalizing molecularly imprinted polymers synthesized by radical polymerization. Polym. Chem. **2020**, 11, 1055-1061. DOI: 10.1039/C9PY01629E.

[23] Yang, J.; Zhang, X.; Mijiti, Y.; Sun, Y.; Jia, M.; Liu, Z.; Aisa, H. A. Improving performance of molecularly imprinted polymers prepared with template of low purity utilizing the strategy of macromolecular crowding. *J. Chromatogr. A* **2020**, 1624, 461155. DOI: 10.1016/j.chroma.2020.461155.

[24] Jia, M.; Yang, J.; Sun, Y. K.; Bai, X.; Wu, T.; Liu, Z. S.; Aisa, H. A. Improvement of imprinting effect of ionic liquid molecularly imprinted polymers by use of a molecular crowding agent. *Anal. Bioanal. Chem.* **2018**, 410, 595-604. DOI: 10.1007/s00216-017-0760-5.

[25] Chen, W. J.; Shang, P. P.; Fang, S. B.; Huang, Y. P.; Liu, Z. S. Origin of macromolecular crowding: Analysis of recognition mechanism of dual-template molecularly imprinted polymers by in silico prediction. J. Chromatogr. A **2022**, 1662, 462695. DOI: 10.1016/j.chroma.2021.462695.

[26] Tan, N.; Chen, C.;Ji, K.; Liao, S.; Liu, Y.; Hu, L.; Ding, Z. Preparation and Properties of Hollow Magnetic Liquid Crystal Molecularly Imprinted Polymers as Silybin Sustained-release Carriers. *Chemistry Select*. **2021**, 6, 9024-9031. DOI: 10.1002/slct.202101786.

[27] Zhang, L. P.; Mo, C. E.; Huang, Y. P.; Liu, Z. S. Preparation of liquid crystalline molecularly imprinted polymer coated metalorganic framework for capecitabine delivery. Part. Part. Syst. Charact. **2019**, 36, 1800355. DOI: 10.1002/ppsc.201800355.

[28] BelBruno, J. J.; A. Richter.; U.J. Gibson. Amazing pores: processing, morphology and functional states of molecularly imprinted polymers as sensor materials. *Mol. Cryst. Liq. Cryst*. **2008**, 483, 179-190. DOI: 10.1080/15421400801905135.

[29] Marty, J. D.; Mauzac, M.; Fournier, C.; Rico-Lattes, I.; Lattes, A. Liquid crystal polysiloxane networks as materials for molecular imprinting technology: memory of the mesomorphic organization. *Liq. Cryst.* **2002**, 29, 529-536. DOI: 10.1080/ 026782 90 11 0068433.

[30] Binet, C.; Ferrère, S.; Lattes, A; Laurent, E.; Marty, J. D.; Mauzac, M.; Weyland, M. Benefit of liquid crystal moieties in the MIP technique. *Anal. Chim. Acta* **2007**, 591, 1-6. DOI: 10.1016/j.aca.2006.12.042.

[31] Binet, C.; Bourrier, D.; Dilhan, M.; Estève, D.;Ferrère, S.; Garrigue, J. C.; Mingotaud, A. F. First approach to the use of liquid crystal elastomers for chemical sensors. *Talanta* **2006**, 69, 757-762. DOI: 10.1016/j.talanta.2005.11.027.

[32] Wei, Q.; Chen, X.; Bai, L.; Zhao, L.; Huang, Y.; Liu, Z. Preparation of liquid crystal-based molecularly imprinted monolith and its molecular recognition thermodynamics. *Chin. J. Chromatogr. (SePu)* **2021**, 39, 1171-1181. DOI: 10.3724/sp.j.1123.2021.01017.

[33] Cieplak, M.; Węgłowski, R.; Iskierko, Z.; Węgłowska, D.; Sharma, P. S.; Noworyta, K. R.; Kutner, W. Protein determination with molecularly imprinted polymer recognition combined with birefringence liquid crystal detection. *Sensors* **2020**, 20, 4692. DOI: 10.3390/s20174692.

[34] Zhang, L. P.; Wei, Z. H.; He, S. N.; Huang, Y. P.; Liu, Z. S. Preparation, charactriza-tion, and application of soluble liquid crystalline molecularly imprinted polymer in electrochemical sensor. *Anal.Bioanal.Chem*. **2020**, 412, 7321-7332. DOI: 10.1007/s00216-020-02866-4.

[35] Palaprat, G.; Mingotaud, A. F.; Langevin, D.; Mauzac, M.; Marty, J. D. Molecularly imprinted cholesteric materials for enhanced enantiomeric separation. *Polymer* **2022**, 243, 124654. DOI: 10.1016/j.polymer.2022.124654.

[36] Yun, Y.H.; Shon, H. K.; Yoon, S. D. Preparation and characterization of molecularly imprinted polymers for the selective separation of 2, 4-dichlorophenoxyacetic acid. J. Mater. Sci. **2009**. 44, 6206-6211. DOI: 10.1007/s10853-009-3863-3.

[37] Del Sole, R.; De Luca, A.; Catalano, M.; Mele, G.; Vasapollo, G. Noncovalent imprinted microspheres: preparation, evaluation and selectivity of DBU template. *J. Appl. Polym. Sci.* **2007**, 105, 2190-2197. DOI: 10.1002/app.26208.

[38] Djamaa, Z.; Lerari, D.; Mesli, A.; Bachari, K. Poly (acrylic acid-co-styrene)/clay nanocomposites: Efficient adsorbent for methylene blue dye pollutant *Int. J. Plast. Technol.* **2019**, 23, 110. DOI: 10.1007/s12588-019-09237-4.

[39] Pavlovic, I.; Barriga, C.; Hermosín, M. C.; Cornejo, J.; Ulibarri, M. A. Adsorption of acidic pesticides 2, 4-D, Clopyralid and Picloram on calcined hydrotalcite. *Appl. Clay. Sci.* **2005**, 30, 125-133. DOI: 10.1016/j.clay.2005.04.004.

[40] Dounya, M.; Maschke, U.; Bouchikhi, N.; Ziani Chérif, H.; Bedjaoui-Alachaher, L. Characterization of swelling behavior and elastomer properties of acrylate polymers containing 2-ethylhexyl and isobornyl esters. *Polym.Bull.* **2022**, 1. DOI: 10.1007/s00289-022-04491-w.

[41] Campbell, S. E.; Collins, M.; Xie, L.; BelBruno, J. J. Surface morphology of spin-coated molecularly imprinted polymer films. *Surf Interface Anal.* **2009,** 41, 347-356. DOI: 10.1002/sia.3030.

[42] Costa, J. C. S.;, Ando, R. A.; Sant'Ana, A. C.; Rossi, L. M.; Santos, P. S.; Temperini, M. L. A.; Corio, P. High performance gold nanorods and silver nanocubes in surface-enhanced Raman spectroscopy of pesticides *Phys. Chem. Chem. Phys*. **2009**, 11, 7491. DOI: 10.1039/B904734D.

[43] Benladghem, Z.; Seddiki, S. M. L.; Dergal, F.; Mahdad, Y. M.; Aissaoui, M.; Choukchou-Braham, N. Biofouling of reverse osmosis membranes: Assessment by surface-enhanced Raman spectroscopy and microscopic imaging .*Biofouling* .**2022**, 38,
852. DOI: 10.1080/08927014.2022.2139610.

[44] Hilal, N.; Kochkodan, V.; Al-Khatib, L.; Busca, G. Characterization of molecularlyimprinted composite membranes using an atomic force microscope. Surf Interface Anal. **2002**, 33, 672-675. DOI: 10.1002/sia.1434.

[45] López, M. D. M. C.; Pérez, M. C.; García, M. S. D.; Vilariño, J. M. L.; Rodríguez, M. V. G.; Losada, L. F. B. Preparation, evaluation and characterization of quercetin-molecularly imprinted polymer for preconcentration and clean-up of catechins. *Anal. Chim. Acta* **2012,** 721, 68-78. DOI: 10.1016/j.aca.2012.01.049.

[46] Chapuis, F.; Pichon, V.; Lanza, F.; Sellergren, B.; Hennion, M. C. Retention mechanism of analytes in the solid-phase extraction process using molecularly imprinted polymers:

application to the extraction of triazines from complex matrices. *J. Chromatogr. B* **2004**, 804, 93-101. DOI: 10.1016/j.jchromb.2003.12.033.

[47] Cao, F.; Wang, L.; Tian, Y.; Wu, F.; Deng, C.; Guo, Q.; Lu, S. Synthesis and evaluation of molecularly imprinted polymers with binary functional monomers for the selective removal of perfluorooctane sulfonic acid and perfluoro octanoic acid. *J. Chromatogr. A* **2017**, 1516, 42-53. DOI: 10.1016/j.chroma.2017.08.023.

[48] Yuan, F. F.; Zhang, R. R.; Ma, X.; Yang, J.; Huang, Y. P.; Liu, Z. S. Cooperation effect of 4-vinylbenzeneboronic acid/methacrylic acid on affinity of capecitabine imprinted polymer for drug carrier. *Eur J Pharm Sci* **2020**, 154, 105476. DOI: 10.1016/j.ejps.2020.105476.

[49] Chen, J.; Wang, L.; Liu, Y.; Chen, L.; Li, X.; Wang, X.; Zhu, G. Highly selective removal of kitasamycin from the environment by molecularly imprinted polymers: Adsorption performance and mechanism. *Colloids Surf. A: Physicochem. Eng. Asp*. **2021**, 625, 126926. DOI: 10.1016/j.colsurfa.2021.126926.

[50] Annamma, K.M.;Beena, M., Design of 2, 4-dichlorophenoxyacetic acid imprinted polymer with high specificity and selectivity. *Mater. Sci. Appl.* **2011**, 2, 131. DOI: 10.4236/msa.2011.23017.

[51] Schwarz, L.; Holdsworth, C. I.; McCluskey, A.; Bowyer, M. C. Synthesis and evaluation of a molecularly imprinted polymer selective to 2, 4, 6-trichlorophenol. *Aust. J. Chem.* **2004**, 57, 759-764. DOI: 10.1071/CH04004.

Table captions

Table 1. Composition of MIP/NIP precursor solutions.

Series	Formulation code	[M]* (mol%)	2,4-D : M : HDDA
1	NIP1	100/0	0 :4: 20
	NIP2	80/20	0 :4: 4
	NIP3	50/50	0 :4: 4
2	MIP1	100/0	1 :4: 20
	MIP2	80/20	1 :4: 4
	MIP3	50/50	1 :4: 4

[M] *: BMA/A6OCB

Table 2. The AFM characteristics of the porous structure of the MIP films

Polymer film	Average roughness (Ra) nm	Root mean squared roughness (RMS) nm	Maximum peak to valley roughness (Rmax) nm
NIP1	1.027 ± 0.04	1.29 ± 0.08	7.26 ± 1.2
MIP1	1.66 ± 0.31	2.09 ± 0.4	11.61 ± 1.8
NIP2	1.62 ± 0.3	2.14 ± 0.5	12.47 ± 3
MIP2	1.82 ± 0.4	2.35 ± 0.6	12.95 ± 3
NIP3	1.87 ± 0.45	2.37 ± 0.6	11.71 ± 3.4
MIP3	1.94 ± 0.2	2.47 ± 0.3	13.31 ± 3.2

Table 3. Selectivity factors for MIP1, MIP2 and MIP3.

MIP films	Selectivity factor
MIP1	0.60
MIP2	0.51
MIP3	0.36

Figures Captions

Figure 1. Chemical structures of (a) n-butyl methacrylate (BMA) (b) 6-(4'-cyanophenyl-4''-phenoxy) hexyl acrylate (A-6OCB), (c) 1,6-hexanediol diacrylate (HDDA), (d) 2,4-dichlorophenoxyacetic acid (2,4-D), (e) phenoxyacetic acid (POAc).

Figure 2. FTIR spectra of BMA, A6OCB (a) and NIP1, NIP2, NIP3 (b).

Figure 3. FTIR spectra of 2,4-D (a) and MIP1, MIP2, MIP3 (b).

Figure 4. Raman Spectra of A6OCB (a) and NIP1, NIP2, NIP3 (b).

Figure 5. Raman spectra of 2,4-D (a), MIP1, MIP2, MIP3 (b) and a zoom of the spectra around 647cm^{-1}(c).

Figure 6. Raman spectra of 2,4D, MIP1, Washed MIP1(a) and a zoom of the spectra around 647 cm^{-1}(b).

Figure7. Raman mapping of MIP 2 (left) and MIP 3 (Right).

Figure 8. Optical micrographs showing the distribution of LC groups in the NIPs and MIPs films. (a,b) NIP1, (c,d) MIP1, (e,f) NIP2, (g,h) MIP2, (I,j) NIP3, (k,l) MIP3. The left column is with parallel analyzer and polarizer, the right column is with crossed analyzer and polarizer.

Figure 9. AFM 3D images (first row) of NIP1, NIP2, NIP3 (a,b,c), and (second row) MIP1, MIP2, MIP3 (d,e,f)

Figure 10. Binding capacities of MIP (1,2,3)/NIP (1,2,3) in the presence of 1mg/ml of 2,4-D solution.

Figure 11. Schematic representation of non-covalent interactions of 2.4-D with the functional monomers, BMA and A6OCB.

Figure 12. Selectivity of MIP (1,2,3) towards 2,4D and POAc.

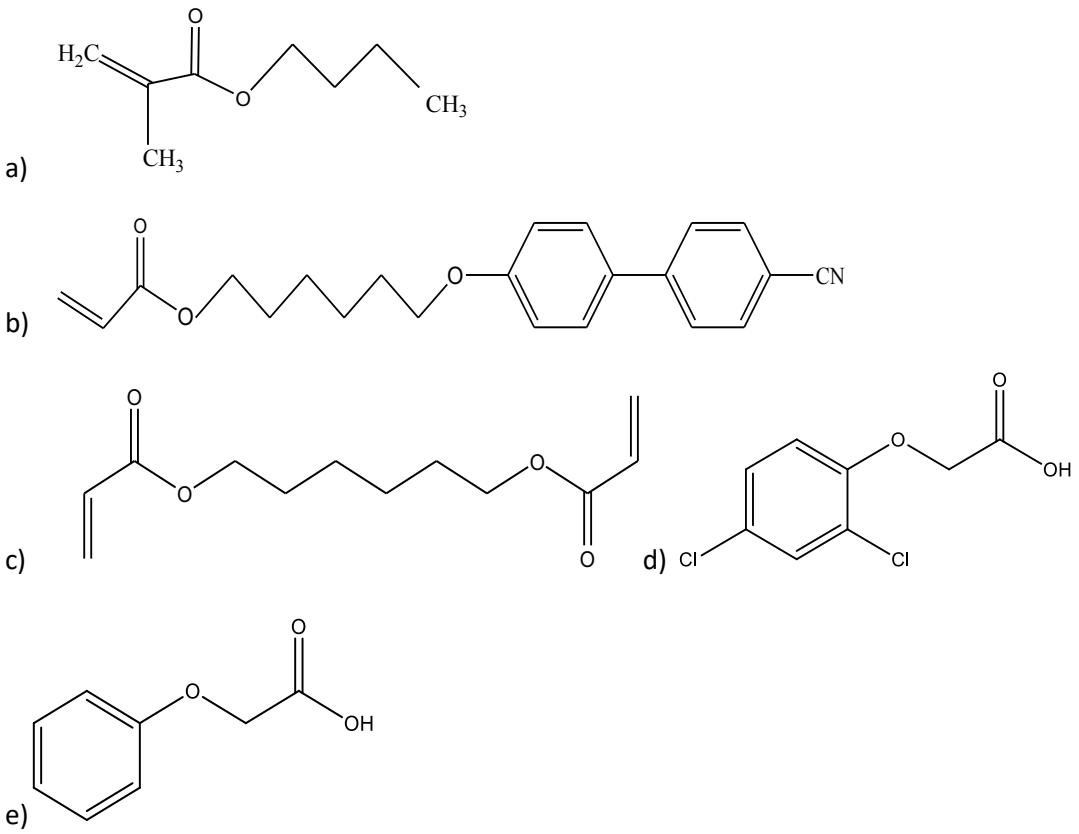

Figure 1. Chemical structures of (a)n-butyl methacrylate (BMA) (b)6-(4'-cyanophenyl-4''-phenoxy) hexyl acrylate (A-6OCB), (c) 1,6-hexanediol diacrylate (HDDA), (d) 2,4-dichlorophenoxyacetic acid (2,4-D), (e) Phenoxyacetic acid (POAc).

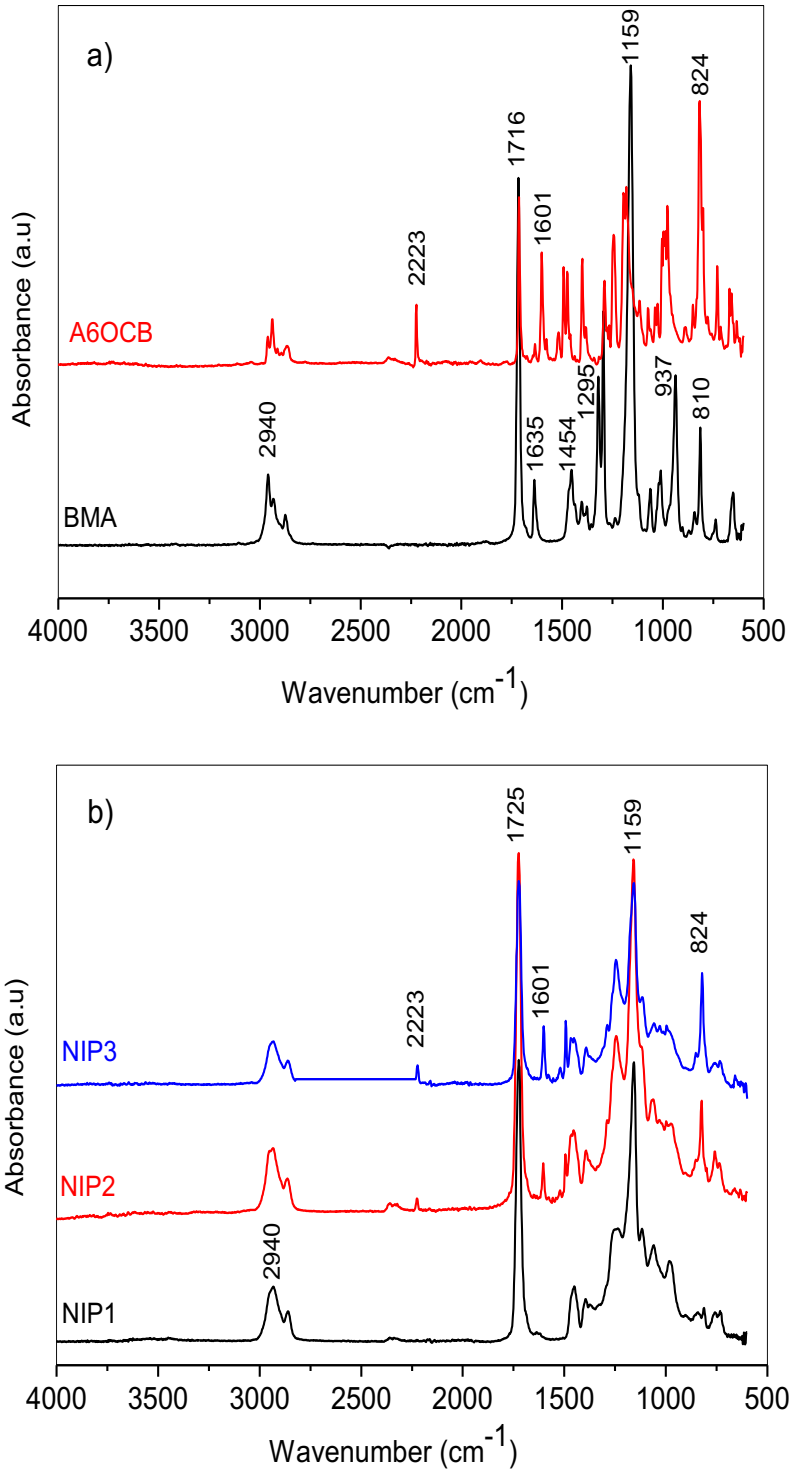

Figure 2. FTIR spectra of BMA, A6OCB (a) and NIP1, NIP2, NIP3 (b).

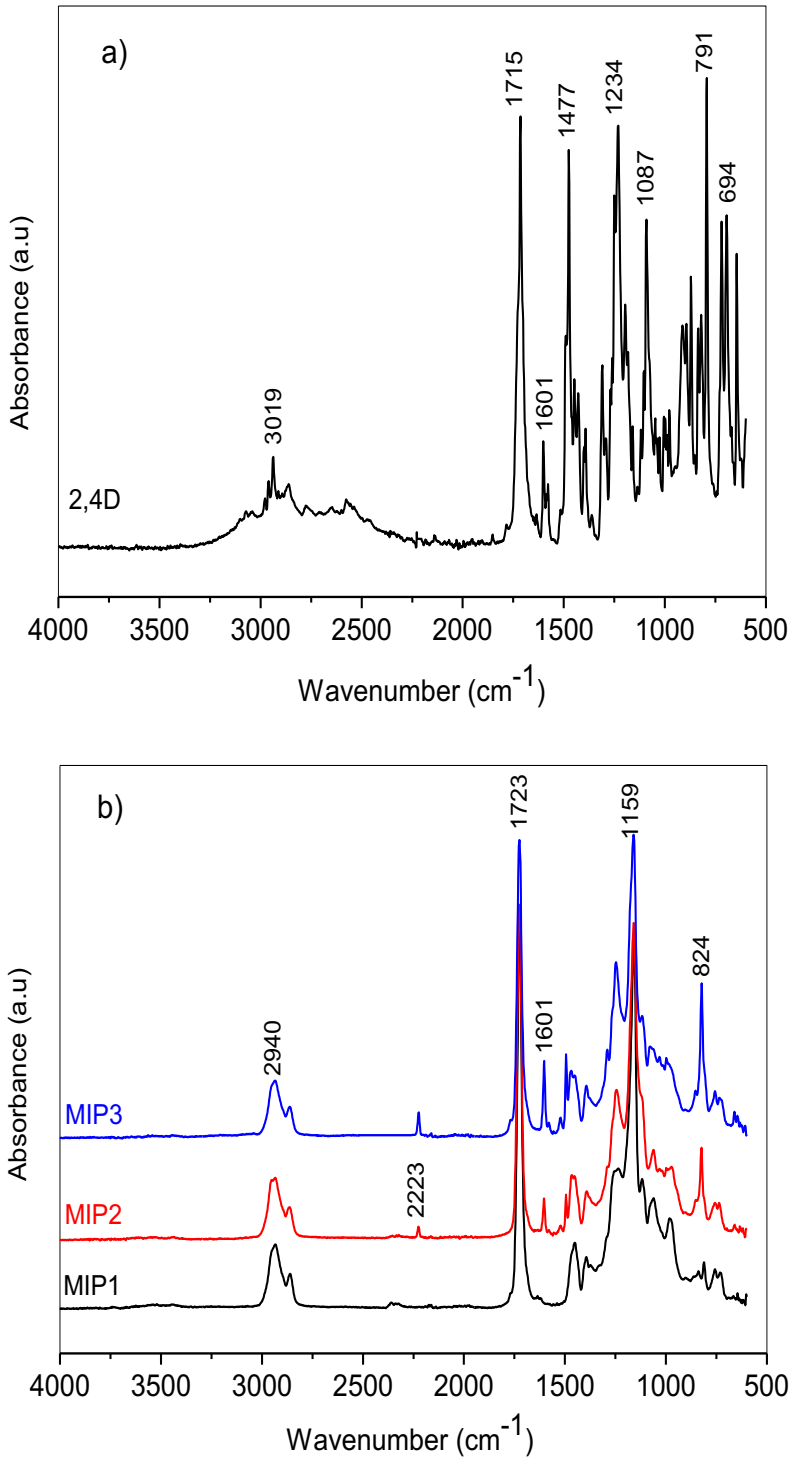

Figure 3. FTIR spectra of 2,4-D (a) and MIP1, MIP2, MIP3 (b).

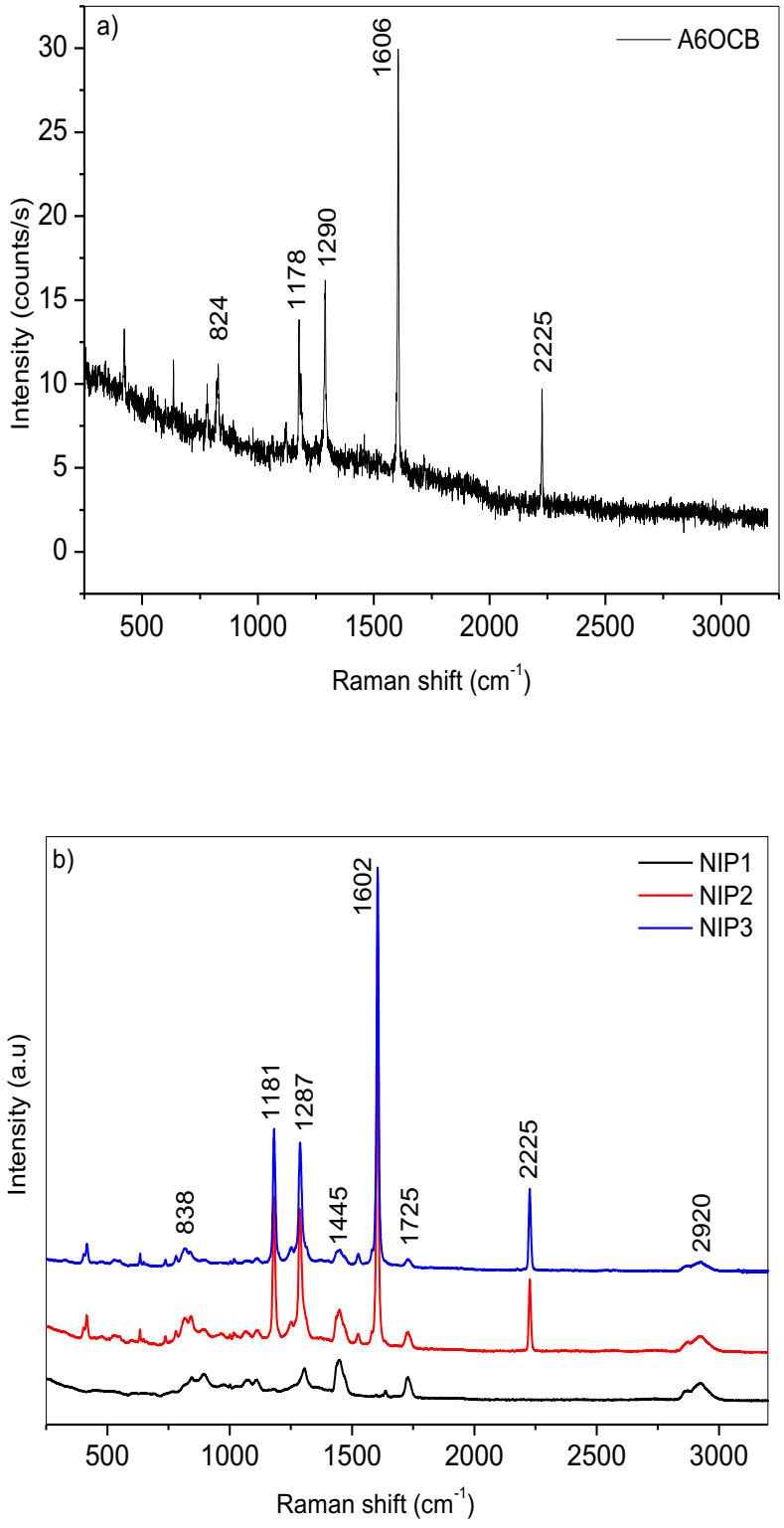

Figure 4. Raman Spectra of A6OCB (a) and NIP1, NIP2, NIP3 (b).

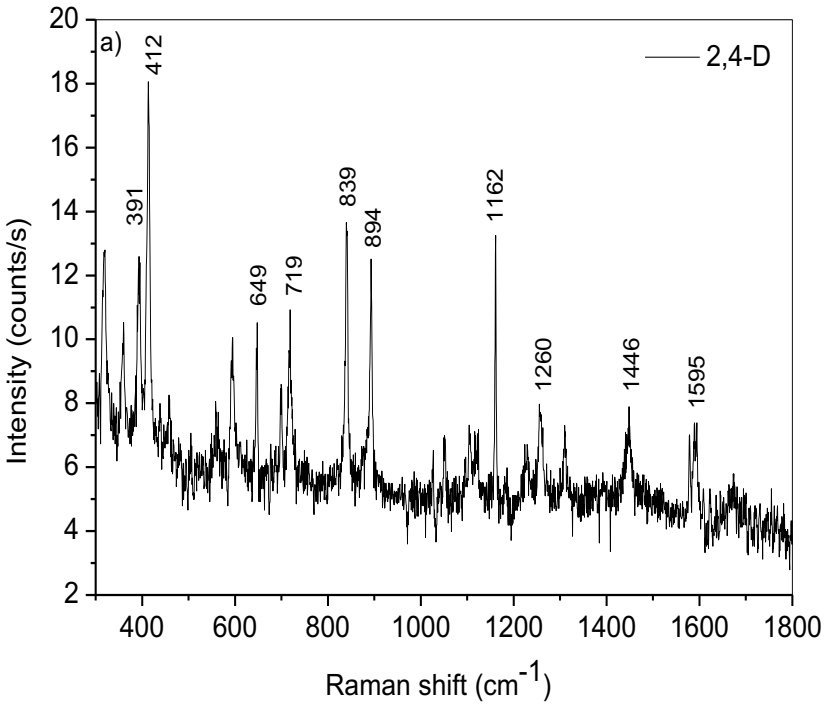
a)
2,4-D
Intensity (counts/s)
Raman shift (cm-1)
412
391
649
719
839
894
1162
1260
1446
1595

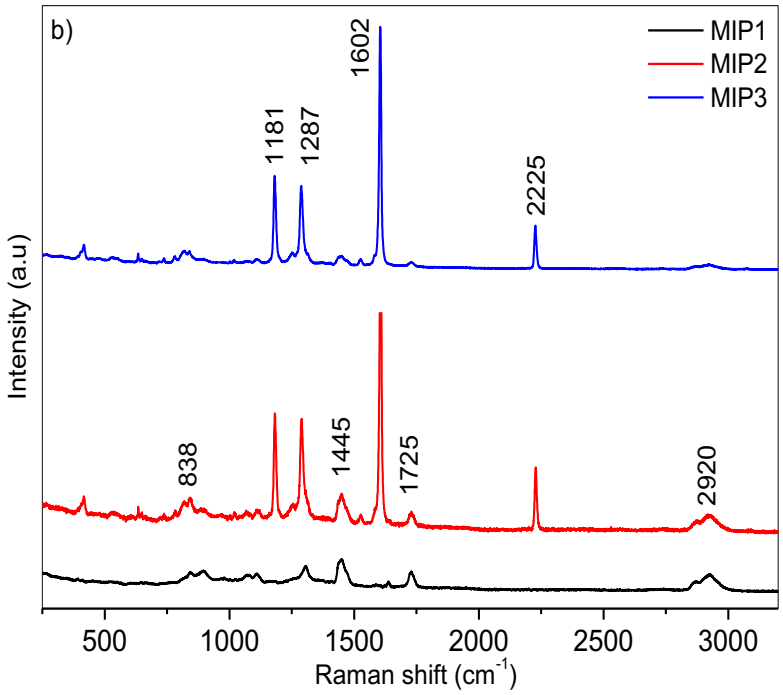
b)
MIP1
MIP2
MIP3
Intensity (a.u)
Raman shift (cm-1)
1602
1181
1287
2225
838
1445
1725
2920

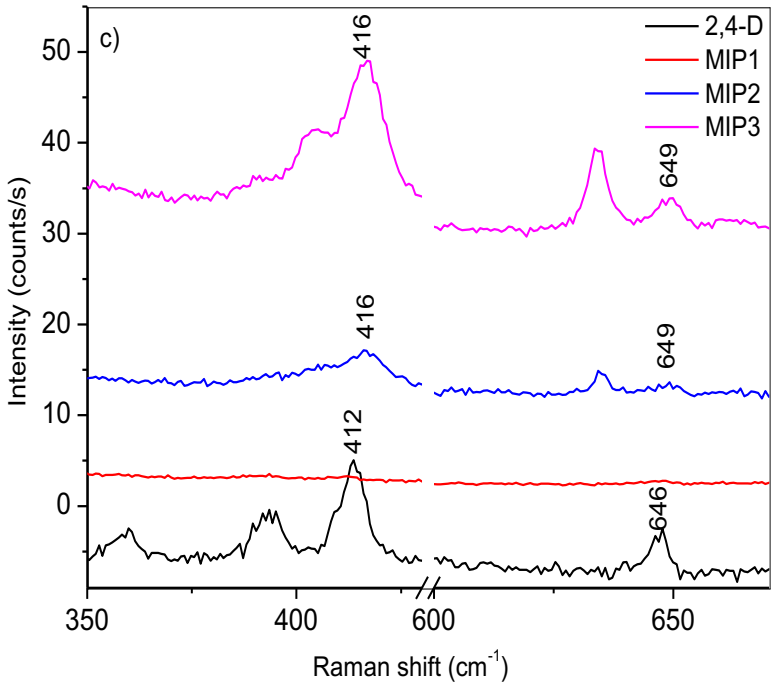

Figure 5. Raman spectra of 2,4-D (a), MIP1, MIP2, MIP3 (b) and a zoom of the spectra around 412 cm^{-1} and 649 cm^{-1}(c).

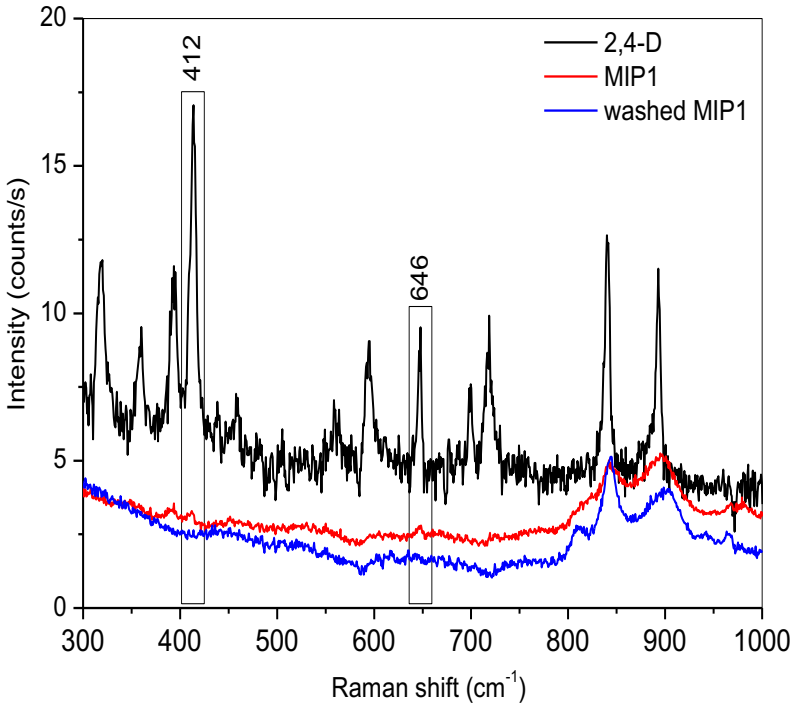

Figure 6. Raman spectra of 2,4-D, MIP1 and washed MIP1 around 412 cm^{-1} and 649 cm^{-1}.

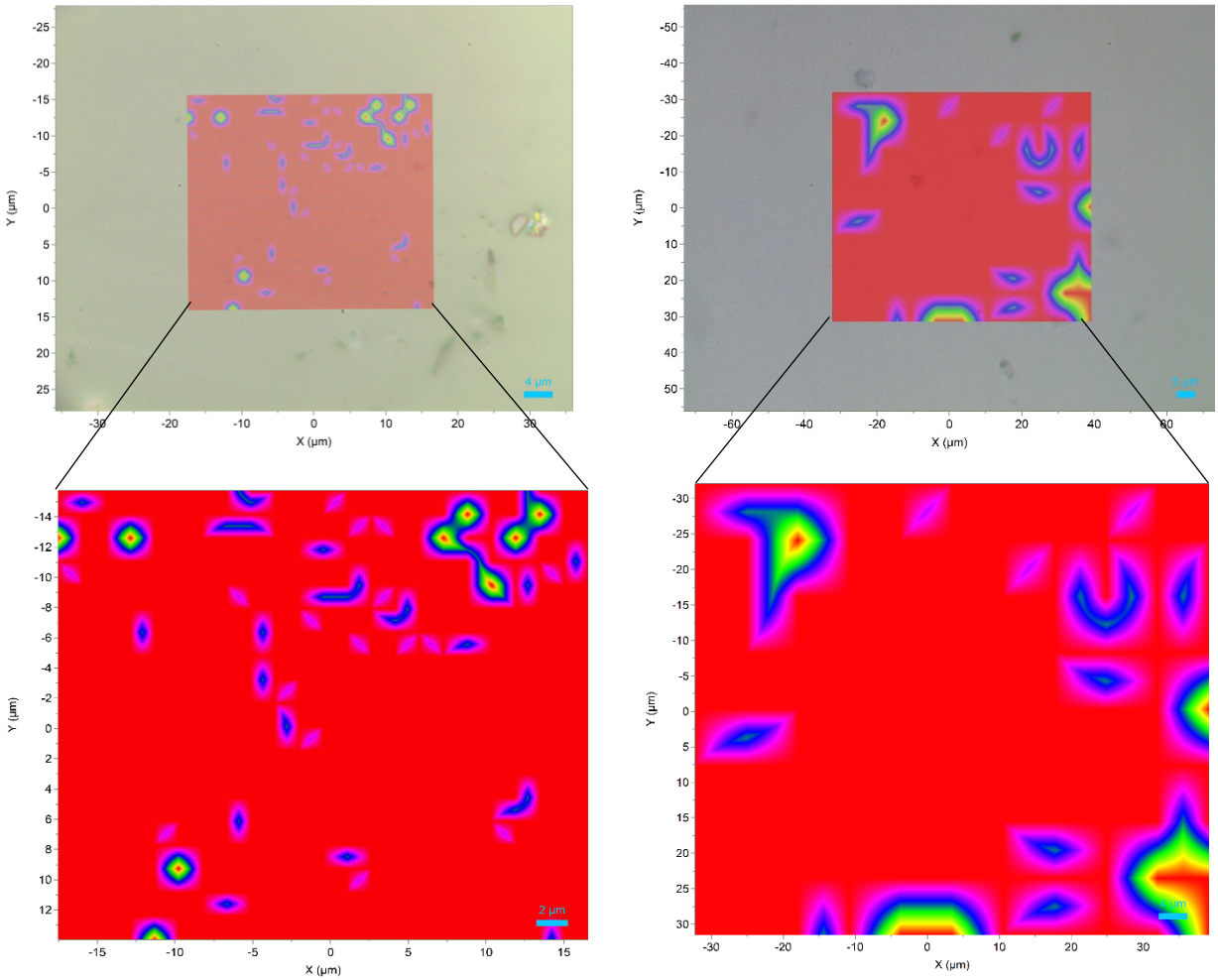

Figure 7. Raman Mapping of MIP 2 (left) and MIP 3 (Right) expressed in terms of their characteristic peaks.

a)

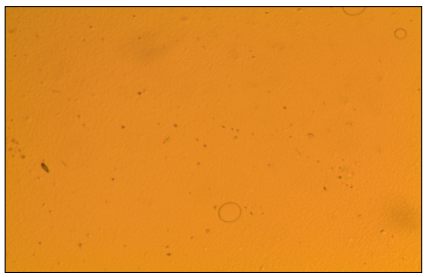

b)

c)

d)

e)

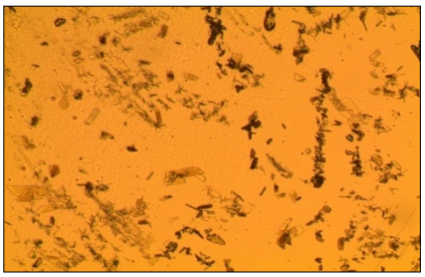

f)

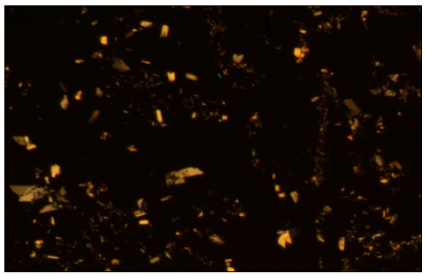

g)

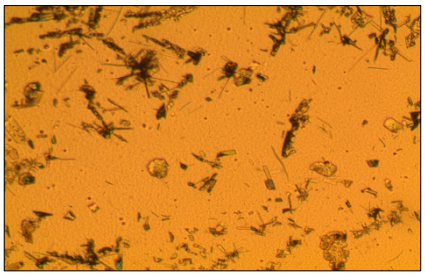

h)

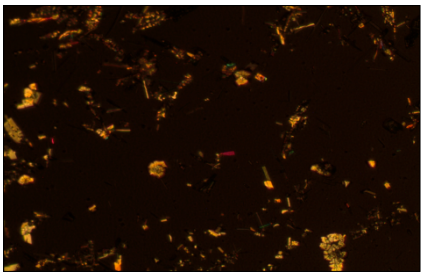

i)

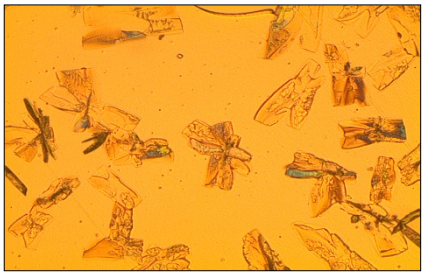

j)

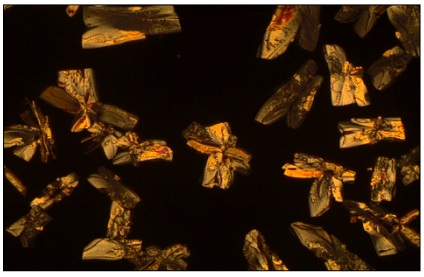

k) l)

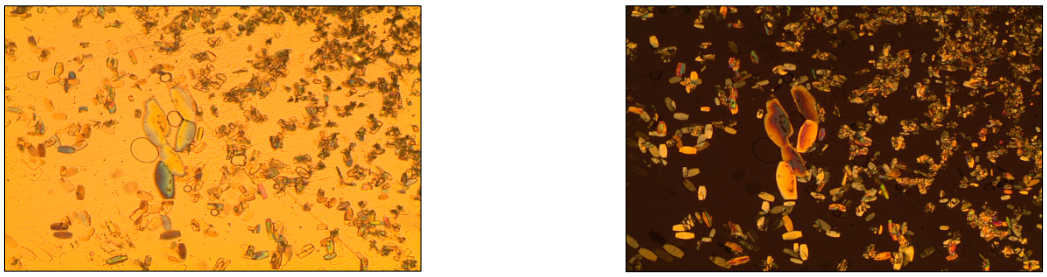

Figure 8. Optical micrographs showing the distribution of LC groups in the NIPs and MIPs films. (a,b) NIP1, (c,d) MIP1, (e,f) NIP2, (g,h) MIP2, (I,j) NIP3, (k,l) MIP3. The left column is with parallel analyzer and polarizer, the right column is with crossed analyzer and polarizer.

a) b) c)

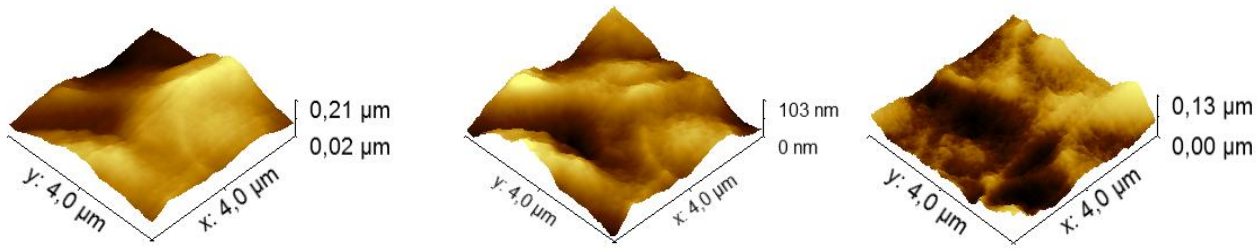

NIP1 NIP2 NIP3

d) e) f)

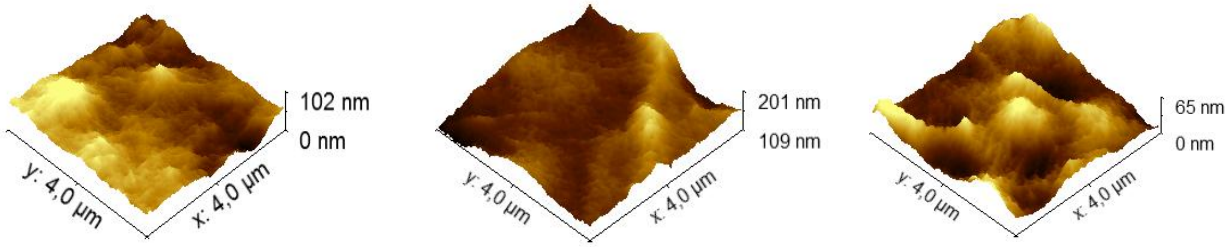

MIP1 MIP2 MIP3

Figure 9. AFM 3D images (first row) of NIP1, NIP2, NIP3 (a,b,c), and (second row) MIP1, MIP2, MIP3 (d,e,f)

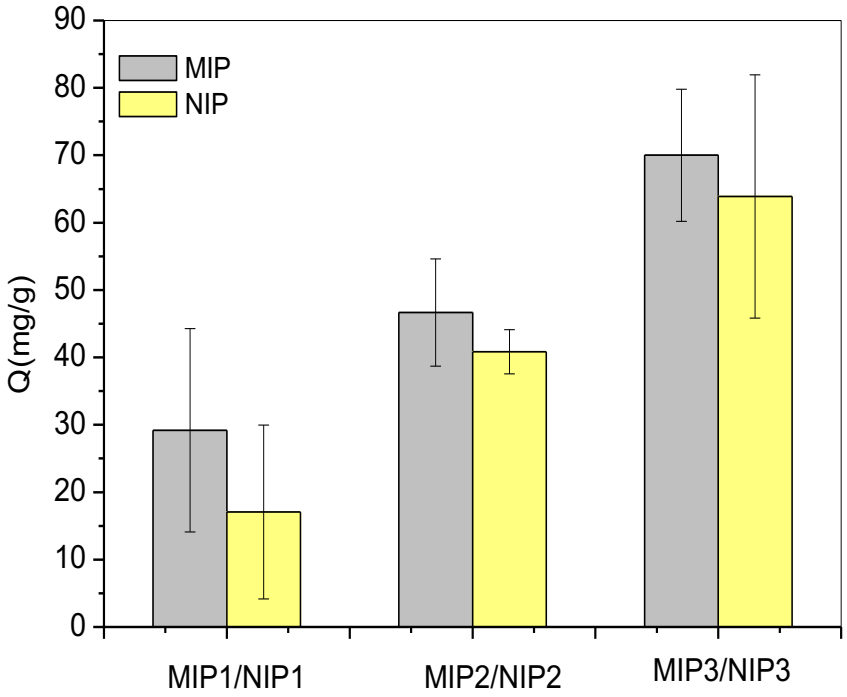

Figure 10. Binding capacities of MIP (1,2,3)/NIP (1,2,3) in the presence of 1mg/ml of 2,4-D solution.

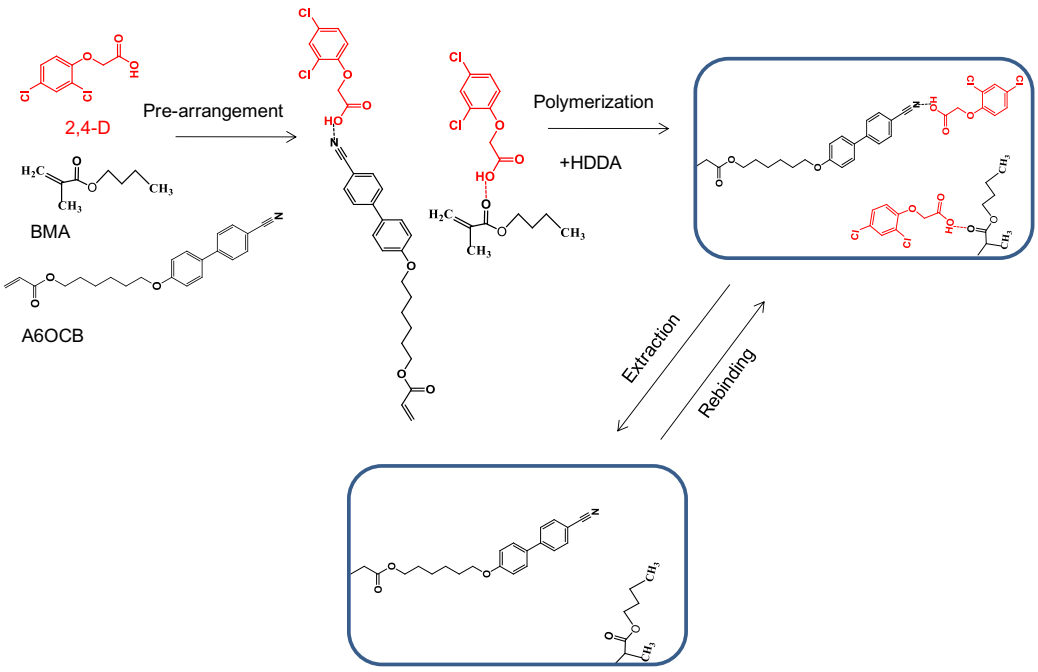

Figure 11. Schematic representation of non-covalent interactions of 2,4-D with the functional monomers, BMA and A6OCB.

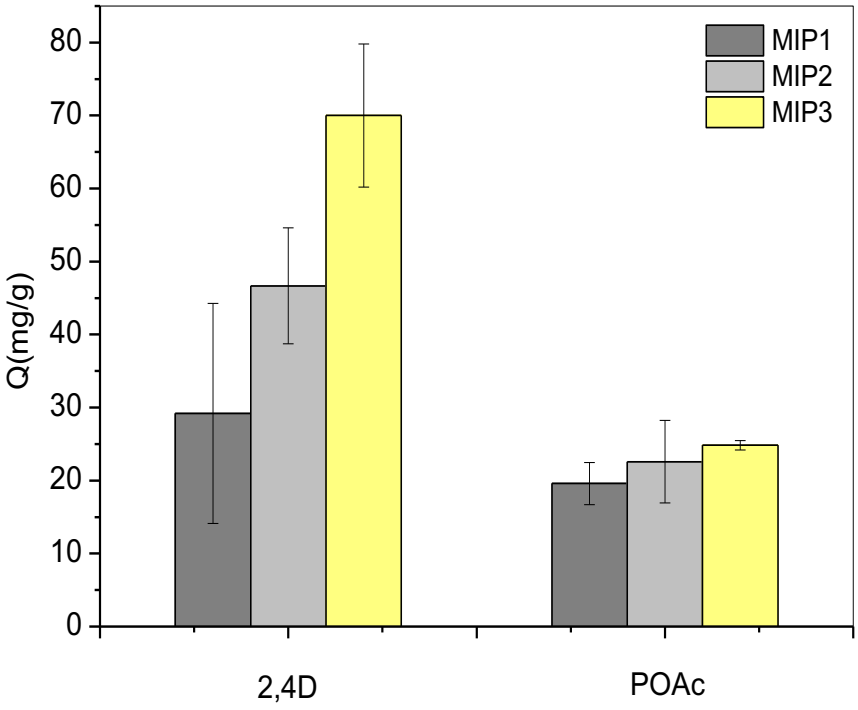

Figure 12. Selectivity of MIP (1,2,3) towards 2,4-D and POAc.